International Journal of Greenhouse Gas Control 55 (2016) 36–41

Contents lists available at ScienceDirect

International Journal of Greenhouse Gas Control

journal homepage: www.elsevier.com/locate/ijggc

IR emitting Dy^{3+} doped chalcogenide fibers for *in situ* CO_2 monitoring in high pressure microsystems

Florent Starecki[a], Sandy Morais[b], Radwan Chahal[a], Catherine Boussard-Plédel[a], Bruno Bureau[a], Fabien Palencia[b], Carole Lecoutre[b], Yves Garrabos[b], Samuel Marre[b,*], Virginie Nazabal[a,*]

[a] Institut Sciences Chimiques de Rennes, Equipe Verres & Céramiques – UMR-CNRS 6226 Université de Rennes 1-CNRS, F-35042 Rennes, France
[b] CNRS, Univ. Bordeaux, ICMCB, F-33600 Pessac, France

ARTICLE INFO

Article history:
Received 29 April 2016
Received in revised form 1 September 2016
Accepted 28 October 2016

Keywords:
Carbon dioxide
Microreactors
Geological lab-on-chip
Optical absorption spectroscopy
Chalcogenide glass and fiber
Rare earth infrared luminescence

ABSTRACT

This paper reports the carbon dioxide detection in silicon-Pyrex high pressure microfluidic devices mimicking geological conditions encountered in deep saline aquifers using an *in situ* infrared optical sensor. The middle infrared source inserted inside the microchannel is based on infrared emission from Dy^{3+} sulfide glass fibers. The broad emission of the Dy^{3+} doping in infrared fibers is used to directly probe the CO_2 thanks to the perfect overlap between the rare earth emission centered at 4.4 μm and the CO_2 absorption band located at 4.3 μm. CO_2 and water were clearly distinguished when using segmented flow on chip at pressures ranging from 4.5 to 6 MPa. These results demonstrate the feasibility of the infrared optical detection of other gases displaying absorption bands in the middle infrared domain for further developments of gas sensors, which can find applications in geological media monitoring and microfluidics.

1. Introduction

Carbon dioxide capture and storage (CCS) is planned to be performed at a large scale, and remains an appropriate long-term option for the reduction of this greenhouse gas concentration in the atmosphere (Lucier and Zoback, 2008). CO_2 can be typically stored in deep geological formations (carbon Geological Storage – CGS) including depleted coal, oil or gas fields or saline aquifers at depths below one kilometer, where the typical temperature and pressure conditions are in the range 30–80 °C and 5–20 MPa (Carr et al., 2005). Mostly demonstrated on shore, CO_2 injection demonstrations were also performed offshore at lower depths, (Mori et al., 2015) to investigate the environmental impact of CO_2 seeping from the seafloor. Indeed, one of the major issue related to these CGS strategies remains the safety of the storage location. It is therefore critical to be able to monitor for a long-term period the entire reservoir, from the wells to the deep underground geological formation in order to detect leaks occurring during the CO_2 injection or appearing during the storage. Such monitoring requires adapted tools working in such conditions (Chadwick et al., 2006). Optical probes have been demonstrated to be candidates of choice for these types of applications. Some example includes the development of a marine sedimentary optical pH profiler (Quieros et al., 2015) to quantify – for instance – the CCS impact on the ocean's acidification. Similarly, an optical fiber system operating at 1.55 μm was recently developed to monitor the CO_2 solubility in aqueous phase above the seafloor (Hingerl et al., 2014). This sensor is based on the CO_2 reaction with the silica fiber cladding, shifting the evanescent wave attenuation. Although the operating pressure was limited to 2.4 MPa in these experiments, it demonstrates the wide interest for these applications. Still, storage areas monitoring at reasonable costs remain a challenge. The requirements and current challenges associated with for such sensors are: the monitoring of wide covered areas (combining multiple measuring heads), a high reliability, a reasonable sensitivity and response time and a compatibility with the pressure and the temperature operating conditions.

The investigation of the processes related to CO_2 storage are mostly performed at reservoir scale, leading to poor understanding of the mechanisms occurring at small pore scale. Meanwhile, microfluidic tools have been extensively used over the past 15 years for chemical synthesis processes (Hartman and Jensen, 2009; Jensen et al., 2014), biology (Duncombe et al., 2015; El-Ali et al., 2006) and materials science (Marre and Jensen, 2010) due to their fast equilibrium times, allowing a better control of the process and less risky manipulations due to smaller volumes. Recently, the

* Corresponding authors.
E-mail addresses: samuel.marre@icmcb.cnrs.fr (S. Marre), virginie.nazabal@univ-rennes1.fr (V. Nazabal).

http://dx.doi.org/10.1016/j.ijggc.2016.10.015
1750-5836/

development of high pressure microfluidics (Marre et al., 2010) has opened ways for researchers to use microfluidics approaches mimicking geological conditions. These geological labs on chip approaches have proved to be powerful methods to study multiphase flows in porous media at lab scale using model microsystems (micromodels) (Morais et al., 2016; Gunda et al., 2011). Such approaches are directly complementary to conventional core scale approaches used by geoscientists (Perrin et al., 2009). Additionally, the advantage of having an optically transparent device provides means to access data, which cannot be obtained through conventional tools (*e.g.* fluid repartition in the porous structure, diffusion properties, solubility measurements, *etc.*), and which can later be used in modelling studies at larger scale. Therefore, experimental works aiming and developing new characterization tools at their implementation into these devices are currently performed (Beuvier et al., 2015). Optical spectroscopy techniques have already been widely used in microfluidics devices including Raman (Liu et al., 2012; Dochow et al., 2013) or UV–visible (Yue et al., 2013). For instance, the quantification of the CO_2 dissolved in water in microfluidic systems was demonstrated using confocal Raman spectroscopy, by comparing the CO_2 Fermi dyad band intensity to the water stretching band intensity (Liu et al., 2012). Another optical system was used to distinguish either water or CO_2 flows in the microchannel, using refractive index variation as detection technique (Burton et al., 2014). The refractive index shift induced by media changes from water to CO_2 is detected on the sensor tip using the light intensity variation due to the Fresnel reflection property. This optical technique - sensitive to medium changes - cannot easily quantify the amount of CO_2 flowing in the microsystem. However, only few studies have reported the development of tools for microscale investigations operating in the near and middle infrared (mid-IR) region, where CCS gases such as CO_2, CO, NO_x or SO_x exhibit absorption bands. Interestingly, this spectral range matches with some rare earth luminescence, which enables developing detection strategies.

In recent years, IR spectroscopy has proved to be a simple, reliable, relatively fast and cost-effective technique for analyzing complex media, creating unique molecular fingerprint. It is used in several research and industrial areas, from quality control to forensic analysis with non-compact IR spectroscopic systems. However, although the use of mid-IR spectroscopy coupled to microfluidics systems has been demonstrated (Perro et al., 2016; Wagner et al., 2011; Kise et al., 2014; Chan et al., 2010; Pan et al., 2004), it is still challenging because the materials parts used during the fabrication of the microreactors have to be transparent in the IR region and have to exhibit good chemical compatibilities with the flowing medium to analyze.

Nevertheless, some *in situ* technological solutions exist and mid-IR spectroscopy based on the use of fibers probes or waveguides (Bureau et al., 2015; Lu et al., 2015) have addressed part of these issues as they can be miniaturized (Kim et al., 2007) and integrated directly within a microreactor. These probes are made of either chalcogenide glasses (Sanghera et al., 2009; Chahal et al., 2016; Singh et al., 2014; Charrier et al., 2012; Ma et al., 2015; Ganjoo et al., 2008; Anne et al., 2009; Starecki et al., 2015; Bureau et al., 2014), germanium (Chang et al., 2012), gallium arsenide or silver halides (Eyal et al., 1996; Charlton et al., 2005). However, to date, most of the microscale devices (microreactors, micromodels) integrated with mid-IR characterization techniques – considering either transparent microreactors options or *in situ* integrated fibers or waveguide ones – are limited to the normal range of pressure and temperature, thus drastically reducing the number of covered applications.

High pressure compatible mid-IR probes could therefore be used for liquid probing or gas sensing including applications in Carbon Capture and Storage since most of the "CCS gases" (CO_2, CO, NOx, SOx, H_2S, *etc.*) exhibit absorption bands in the mid-IR domain.

IR optical detections are commonly performed by means of black body sources, temperature dependent, with low brightness and strongly influenced by the surrounding. In case of geological probes and microfluidic systems, excitation sources could be favorably replaced by trivalent rare earths ions 4f-shell transitions generating light from UV to mid-IR, depending on their host and intrinsic energy scheme. Glasses with low phonon energy are required to ensure the infrared optical transmission and the rare earth emission efficiency. Among some other candidates, the germanium based sulfide glasses fulfil these requirements. These rare earth (RE) doped glasses are providing low costs mid-IR sources, at discrete wavelengths with emission bandwidth of at least 100 nm due to distortions of the electrical field in a glass matrix. Such characteristics outperform blackbody sources in terms of fluency and compactness, and make these sources much cheaper than infrared supercontinuum lasers, showing promising results in developing new mid-IR laser sources (Kubat et al., 2014). These RE fiber sources are well suited for IR absorption spectroscopy, while meeting the concerns of miniaturization for their further integration into microfluidic systems.

We demonstrate in this study an *in situ* mid-IR optical probe to detect carbon dioxide in high pressure microreactors. The presence of CO_2 is directly detected by means of Dy^{3+} sulfide glass fiber luminescence. We had previously demonstrated that the Dy^{3+} doped GaGeSbS fiber luminescence can be successfully used for the CO_2 gas detection at low pressure. For this specific application, the CO_2 detection threshold was fixed in the range of 400–1000 ppm. This optical sensor exhibits a good temporal response and time stability, a very high robustness suitable for efficient commercial sensor. Additionally, some field operations have been presented and consisted in measurements performed in 100 m deep wells, making this macroscopic optical sensor suitable for on-the-field operations in order to monitor geological reservoirs (Starecki et al., 2015). One of the main challenge was to develop a Dy^{3+} mid-IR sensor allowing *in situ* measurement under high pressure in microreactors. After discussing the design and the microfabrication procedure of the microreactor along with the detector principle, the integration of the mid-IR optical probe into the microfluidic device will be presented. The detection of either water or carbon dioxide is then demonstrated in dynamic conditions and the potentialities of this detector are discussed.

2. Materials and methods

2.1. High pressure microreactors and set-up

Among the existing on chip microfluidic devices capable of handling high pressure, the silicon/Pyrex microreactors were used in here (Marre et al., 2010). The flexible microfabrication of silicon through photolithography, wet etching and further anodic bonding to Pyrex allows designing proper geometries to implement fluid analysis monitoring tools, such as optical fibers. The general microreactor design is shown in Fig. 1.

It consists of a U-shape microchannel (width, w = 300 μm, depth, d = 200 μm) implemented with a detection area aiming at positioning the optical fibers thanks to two perpendicular guiding channels (w = 350 μm, d = 200 μm). The microreactor was integrated into a general set-up consisting of two high pressure piston pumps (ISCO 100DM), a coflow generating system (a small capillary inserted in a larger one through a T-junction), which was used to generate CO_2/water segmented flows upstream the microreactor. A back pressure regulator (BPR) was placed downstream to control the pressure in the range 4.5–6 MPa. An additional on/off valve was mounted between the inlet and outlet of the microreactor

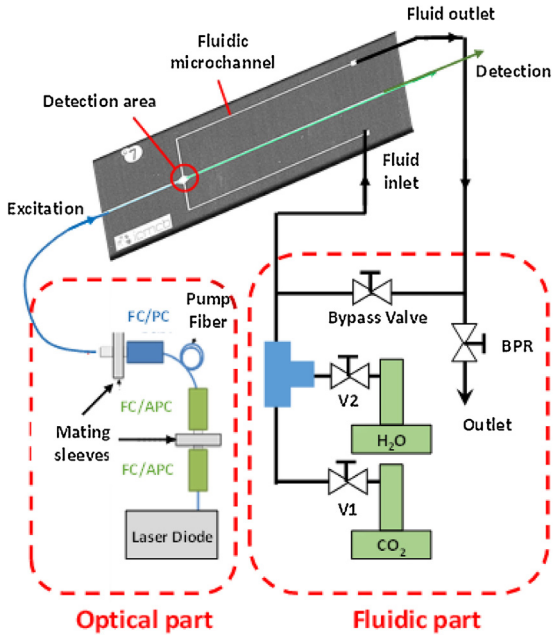

Fig. 1. General design of the microreactor and overall set-up including the optical part and the fluidic part.

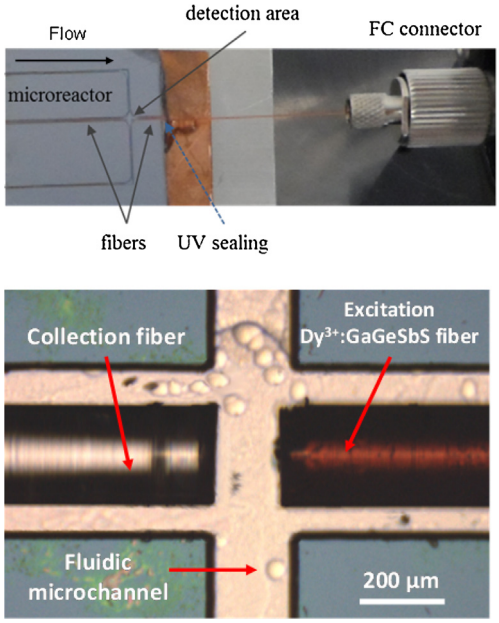

Fig. 2. (Top) Picture of the full device and (Bottom) enlargement of the detection area, showing the fibers positioning.

to bypass the system when working in stop-flow mode. During these experiments, the operating temperature of the microreactor was regulated by a thermoelectrical device (TEC module) mounted below the chip and controlled by a Thorlabs TED200C temperature controller. A thin copper plate is placed between the chip and the TEC module to ensure a homogeneous heating of the chip.

2.2. Optical detection system implementation

The excitation and collection fiber are first inserted into the guiding microchannels and their alignment is optimized using XYZ translation stages, then the fibers are sealed using an UV curable resin Kloé K-PuM01 (Fig. 2 top). The distance between the two

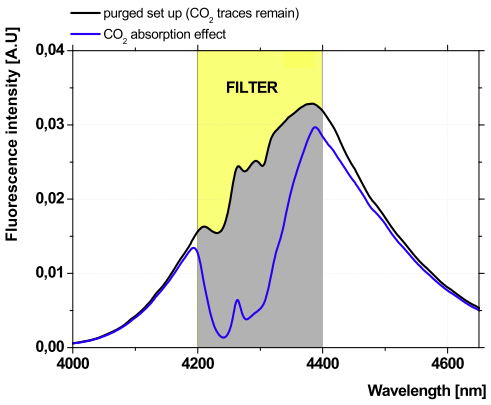

Fig. 3. Dy^{3+}:GaGeSbS emission band centered at 4.4 µm, with the CO_2 absorption band at about 4.23 µm (grey). Yellow: transmission window of the filter used to measure the CO_2 absorption (centered at 4.23 µm). (For interpretation of the references to colour in this figure legend, the reader is referred to the web version of this article.)

fibers can vary in the range 300–500 µm, depending on the experiment. The collection fiber can be a non-doped chalcogenide fiber or a fluoride fiber (Le Verre Fluoré©) (transparent fiber on Fig. 2 bottom).

The output fiber signal is collimated by a first CaF_2 lens, and passes through a Spectrogon BP-4300-200 filter. Its transmission overlaps the 4.3 µm Dy^{3+} doped sulfide glass emission affected by the CO_2 absorption (Fig. 3). Fig. 3 was obtained using a monochromator and allows the proper selection of the central wavelength and bandwidth of the filter.

After the filter, a second lens focuses the IR signal on the detector, which is a liquid nitrogen cooled InAsSb chip (Hamamatsu P11120-901 and C4159-01 preamplifier). The electrical signal is then recorded using a NI-USB-6341 data acquisition device.

The *in situ* IR optical probe is monitored though a LabVIEW application, controlling the pump laser diode modulation and recording the output signal from the InAsSb detector. The optical pump signal is modulated at a frequency of 21 Hz, which is far below the frequencies of the Dy^{3+} luminescence and the InAsSb rise times. The data accumulation and simultaneous processing lasts 100 ms, which corresponds to the detector temporal resolution. The noise reduction is performed on the raw signal by applying a Stavisky-Golay filter.

2.3. Dy: GaGeSbS fibers preparation

The single index fiber is a $Ga_5Ge_{20}Sb_{10}S_{65}$ doped with 1200 ppm of Dy^{3+}. The preform was prepared using conventional melting and quenching methods and high purity raw materials (5N, and 3N for the rare earth sulfides). Once the glass preform was annealed, chalcogenides fibers were drawn. The fiber diameter was adjusted to 180 µm to ensure further embedding in the microfluidic device. More details about the preform synthesis and the fiber drawing of these materials are given in the following references (Charpentier et al., 2013; Moizan et al., 2008).

The excitation fibers were then dip coated in a KLOÉ K-Cl-050 UV curable component on a homemade dip-coating device derived from a fiber drawing apparatus. The coating is the appropriate answer for addressing both the mechanical and the optical losses issues. It was performed soon after the drawing in order to limit the surface alteration by oxygen and water. A 15 ± 2 µm coating is deposited around the fiber, improving the mechanical properties of chalcogenide fibers. Indeed, these fibers intrinsically have a weak strain resistance and low bending radius compared to silica fibers. The coating improves these features, making the fiber more

resistant to handle when performing technical stages such as connection, polishing and insertion in the microsystem. Additionally, it not induces extrinsic infrared optical losses since the resin exhibits a high transmission in the 3–5 μm range. Moreover, the coating also prevents from an optical leakage due to the evanescent coupling into the silicon part of the microfluidic reactor, which presents an upper optical index leading to higher optical losses.

The optical pumping was performed by a Lumics Lu0915T090 laser diode, tuned at 918 nm. The Dy^{3+} sulfide fibers (180 μm) were operating safely considering a 2.2 W pumping power using a silica fiber (105 μm) for injection. The pumping diode was isolated from optical damage by using two FC/APC connectors to prevent from a pump back-reflection in the laser diode. Although accurate power measurements have not been conducted on this specific fiber, previous laboratory tests on comparable fibers performed with IR adapted optical collimators have shown few hundreds of microwatts at their output emitted from the 4.3 μm Dy^{3+} transition. However, it is not yet possible to embed these collimators into the microsystem. Therefore, high coupling losses can be expected at the inlet of the collection fiber. Indeed, the numerical aperture of the emitting fiber is at maximum because of its high refractive index, while the collection fiber has a lower numerical aperture partially rejecting light. Once coated, these fibers are then polished on both ends using several Al_2O_3 polishing plates. One end is mounted in a FC connector; the other could be then inserted into the microfluidic device.

3. Results

3.1. Mid-infrared fluorescence

From the 918 nm ($^6F_{7/2}$) optical pumping, the Dy^{3+} luminescence shows several emission bands at 1.3, 1.8, 3.0 and 4.3 μm (Starecki et al., 2015). This latter emission line is here used to probe the CO_2 absorption band. On Fig. 3, the 4.1–4.6 μm luminescence is presented, with the CO_2 absorption effect at 4.23 μm. The principle of the CO_2 optical detection lies on the Beer-Lambert's absorption law, by measuring the transmitted infrared light intensity in this wavelength domain. Indeed, the optical signal intensity decreases as the CO_2 concentration increases.

3.2. Carbon dioxide detection

After setting the temperature to 25 °C, the bypass valve was closed and the microfluidic device was first pressurized with water up to 6 MPa. A first set of experiments has consisted in flowing gaseous CO_2 (50 μL min^{-1}) at a pressure of 5 MPa. The valve V1 was opened, while the valve V2 was closed (Fig. 1). As the water in the system is purged, the pure CO_2 signal was recorded. Closing valve V1 and opening valve V2, while keeping the pressure and flow rate constant allows switching from a CO_2 to a H_2O injection; therefore, the signal corresponding to the transition from pure CO_2 to pure water can be observed (Fig. 4).

The pure CO_2 signal level corresponds to a higher 4.3 μm absorption coefficient than for pure water. As the water slowly flushes the CO_2 out of the detection area, the transmitted infrared signal raises to reach a higher value. As seen on Fig. 4, the transition corresponds to the CO_2/water interface displacement through the detection volume.

The Beer-Lambert's absorption law describes the transmitted signal as an exponential function of the absorption coefficient along the optical path (Eq. (1)). The intensities and absorption coefficients hereafter are implicitly linked to the wavelength domain defined by the bandpass filter (Fig. 3).

$$I/I_0 = exp\,[-\alpha \cdot l_{cell}] \quad (1)$$

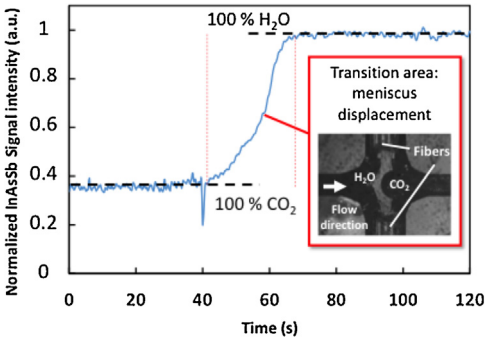

Fig. 4. Pure water and CO_2 electrical signals out of the InAsSb preamplifier (25 °C, 5 MPa).

With α being the global attenuation coefficient per length unit and l_{cell} the distance between the two fibers. This attenuation coefficient also implicates the presence of water. Indeed, liquid water exhibits an absorption coefficient of ~270 cm^{-1} (Hale and Querry, 1973), therefore, both the contributions of CO_2 and water are measured (Eq. (2)).

$$\alpha = \alpha_{CO2} + \alpha_{H2O} \quad (2)$$

At pressure p = 5 MPa and beyond, the absorption coefficient of the gaseous carbon dioxide is higher than the one of liquid water. At such pressures, liquid water compression is about 1%, and can be neglected. In this spectral range, the global absorption coefficient α (Eq. (2)) is then lower in the case of pure water than of gaseous CO_2, the substitution of water by carbon dioxide therefore results in an increase of the absorption coefficient. More interestingly, since the concentration of molecules in the optical path is proportional to the fluid density and pressure, this IR optical probe could turn into a pressure sensor in the case of pure gaseous CO_2, through density determination at a known temperature in stop flow mode. The carbon dioxide concentration is depending on the Signal/Noise ratio, therefore, a proper calibration procedure is required to explore the full potentialities of this IR probe. Indeed, when considering the maximal absorption peak of CO_2, the transmission is equal to zero, (between 4.2 and 4.35 μm). However, at longer wavelength (λ ~ 4.4 μm) the system is transmitting, allowing measuring a wide range of CO_2 concentrations by using a suitable calibration. Compared to the signal transmitted in the air, the remaining intensity is here about 1% when the fluids are installed in the microsystem. Moreover, the Fresnel reflection losses at the fiber/fluid interfaces is about 0.31 dB (at 4.3 μm: fiber index = 2.23 and water index = 1.34).

In a second set of experiments, we investigated the detection system under dynamic flow conditions. Similarly to the previous experiment, the system was first pressurized at p = 5 MPa with water with the by-pass valve being closed. Once the equilibrium was reached and the whole system pressurized, valve V1 and valve V2 were opened, while the two pumps were set to constant flow operation mode (Q_{water} = 100 μL/min; Q_{CO2} = 50 μL/min), the co-flow system generates CO_2/H_2O segmented flow in the microfluidic device, as previously demonstrated (Marre et al., 2009). By adjusting the ISCO pumps flow rates, the size of the CO_2 bubbles in the water flow could be controlled. The ability of the IR probe to detect the presence of CO_2 bubbles was tested, and reported on Fig. 5.

By coupling the optical visualization of the flow and the IR detection signal with the fibers probe, additional information concerning the nature of the fluid passing through the detection area can be gained within a single experiment. Indeed, electrical signals below 4 V could be attributed to the carbon dioxide, while voltage at ~16 V reveals the presence of water. Sorting these measurements can generate feedback information for processes monitoring and control.

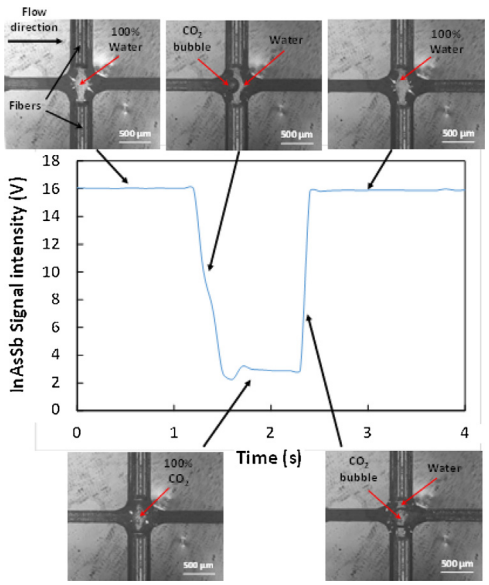

Fig. 5. InAsSb signal intensity and optical visualization of a CO_2 bubble passing through the detector zone.

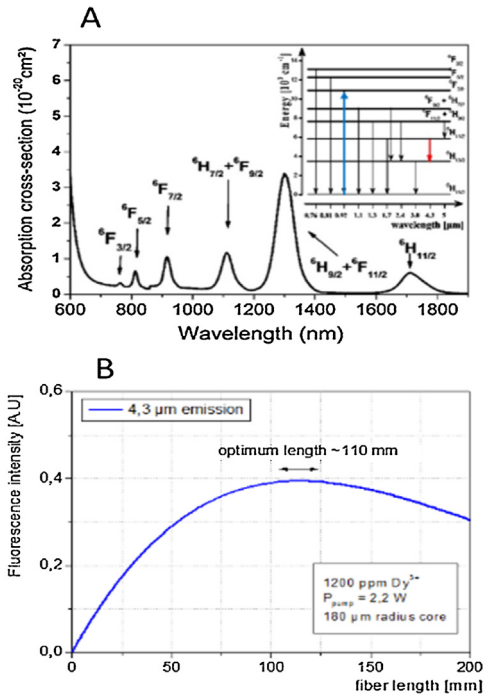

Fig. 6. (A) Dy^{3+}: $Ga_5Ge_{20}Sb_{10}S_{65}$ absorption spectrum and Dy^{3+} energy diagram (inset) (B) expected relative output power as a function of the fiber length.

4. Discussions

The optical properties of the material used for the fiber coating was carefully selected. Its high transparency in the 3.5–5 μm region is leading to a low evanescent wave attenuation. Thus, such a core-clad refractive index contrast (fiber: 2.23 and resin: 1.5) ensures a low penetration depth of the evanescent field (about few hundreds of nanometers). For these coated chalcogenide fibers, an optimum polishing quality is required for an efficient coupling avoiding heat generation at the interface and further fiber burning. With a particular care accorded to these polishing steps, a 2.2 W pumping power was injected in the chalcogenide fiber with a 50% duty cycle.

The cross-section calibrated absorption spectrum of the Dy^{3+}: $Ga_5Ge_{20}Sb_{10}S_{65}$ is reported in Fig. 6A. The 4.3 μm emission of the Dy^{3+} corresponds to its $^6H_{11/2} \rightarrow {}^6H_{13/2}$ transition (Fig. 6A inset), which efficiency η depends on the phonon energy distribution of the glass matrix. More details about the spectroscopic properties of Dy^{3+}: $Ga_5Ge_{20}Sb_{10}S_{65}$ materials can be found in the following reference (Starecki et al., 2015). An appropriate doping level reaches a beneficial compromise between a good pumping beam absorption, the preservation of the emission efficiency from concentration quenching effects and the fiber manufacturing with suitable optical losses. These conditions are typically fulfilled for 1200 ppm Dy^{3+}-doped sulfide fibers.

In such wave guiding optical fibers, the 4.3 μm Dy^{3+} luminescence turns into an Amplified Spontaneous Emission (ASE) phenomenon. From a given dopant concentration (here: 1200 ppm) and considering the maximum pumping power, which could be safely injected within the fiber, the ASE modelling shows that a maximum output power would appear at a given length (Pelé et al., 2015). Briefly, the model consists in calculating the absorbed fraction of the pump and the generated infrared flux in each slice of the fiber, as a function of spectroscopic properties such as the fluorescence lifetimes, the branching ratios, and the absorption or emission cross sections. On Fig. 6B, this 2.2 W pumped, 1200 ppm and 180 μm core radius emitting fiber would reach its maximum output power for a 110 mm length.

Due to their 2.25 refractive index, these chalcogenide fibers have a high numerical aperture (NA), even with the polymer coating. The high beam divergence is leading to some coupling losses, which would increase as the distance between the fibers in the detection area is increasing. Short distances must be preferred, and the optimized distance between the two fibers is typically in the range 350–450 μm, in accordance with our experimental values.

Considering the microreactors, the assembly presented in Figs. 1 and 2 are stable for pressures up to 7 MPa, and temperatures below 50 °C. Nevertheless, further improvement of the microfluidic device design and the fluidic connections should allow operating the system up to 15 MPa, as already reported for similar systems with insertion/gluing of capillaries instead of fibers (Couto et al., 2015).

Overall, this IR optical sensor proved to be efficient to detect pressurized carbon dioxide in water. Moreover, the IR probe can also be used to detect water traces using the 2.8 μm fluorescence of the Dy^{3+}: sulfide glass, simultaneously. In this objective, a 3.0 μm bandpass filter could be used to isolate the dysprosium $^6H_{13/2} \rightarrow {}^6H_{15/2}$ emission band. Unlike liquid water at 4.3 μm, the carbon dioxide is quite transparent for this specific wavelength. Thus, water traces quantification is possible in pure carbon dioxide using multi-wavelength detection heads with the same setup.

5. Conclusions

We have presented here the first demonstration, to our knowledge, of an *in situ* CO_2 mid-IR detection probe integrated within a high pressure microfluidic system simulating geological conditions encountered in deep aquifers. The probe itself consists of an embedded rare earth doped chalcogenide fiber, which was used to detect the presence of dense CO_2. This IR optical probe is able to distinguish if either carbon dioxide or water is flowing in the detection area. With its 100 ms sampling frequency, this detector can also be used in dynamic flow mode.

More generally, optical fibers made of rare earth doped chalcogenide glasses are a promising route for detecting (bio)-chemical species presenting optical absorption bands in the middle infrared. Yet, the rare earth doped chalcogenide fibers offer a low cost, efficient and versatile solution; especially for optical gas detection. The combination of an affordable pumping source, an adapted rare earth with enough emission efficiency in the mid-IR and absorption band of gas molecules must exist. The IR optical sensor design is here adapted for high pressure microfluidic devices, with a polymer coating deposited on the chalcogenide fiber for an easier integra-

tion and prevention of optical leakages. Besides microfluidics, this probe could be easily adapted to high pressure geological media monitoring. Beyond this simple detection of water and CO_2, this proof of concept demonstration opens avenues towards the *in situ* infrared optical detection of other (bio)-chemical species featuring absorption bands in the middle infrared domain. Depending on the targeted applications, further developments of gas sensors can be lade by adapting the doping elements in order to find applications in geological media monitoring and microfluidics.

Acknowledgements

We authors wish to thank the ANR for funding this work through the CGSμLab-ANR-12-SEED-0001-01 project and ADEME for PhD funds. We also gratefully thank Le Verre Fluoré Company for the fluoride fiber samples tested during this work.

References

Anne, M.L., Keirsse, J., Nazabal, V., Hyodo, K., Inoue, S., Boussard-Pledel, C., Lhermite, H., Charrier, J., Yanakata, K., Loreal, O., Le Person, J., Colas, F., Compere, C., Bureau, B., 2009. Chalcogenide glass optical waveguide for infrared biosensing. Sensors 9, 7398–7411.

Beuvier, E.-A.C.T., Kwasniesky, P., Marre, S., Lecoutre, C., Garrabos, Y., Aymonier, C., Calvignac, B., Gibaud, A., 2015. Implementation of in situ SAXS/WAXS characterization into silicon/glass microreactors. Lab Chip 15, 2002–2008.

Bureau, B., Boussard, C., Cui, S., Chahal, R., Anne, M.L., Nazabal, V., Sire, O., Loreal, O., Lucas, P., Monbet, V., Doualan, J.L., Camy, P., Tariel, H., Charpentier, F., Quetel, L., Adam, J.L., Lucas, J., 2014. Chalcogenide optical fibers for infrared sensing. Opt. Eng., 53.

Bureau, B., Boussard-Pledel, C., Troles, J., Nazabal, V., Adam, J.L., Doualan, J.L., Braud, A., Camy, P., Lucas, P., Brilland, L., Quetel, L., Tariel, H., 2015. In: Kalli, K., Kanka, J., Mendez, A. (Eds.), Micro-Structured and Specialty Optical Fibres Iv, vol. 9507.

Burton, G., Melo, L., Warwick, S., Jun, M., Bao, B., Sinton, D., Wild, P., 2014. Fiber refractometer to detect and distinguish carbon dioxode and methane leakage in the deep ocean. Int. J. Greenh. Gas Control 31, 41–47.

Carr, T.R., Merriam, D.F., Bartley, J.D., 2005. Use of relational databases to evaluate regional petroleum accumulation, groundwater flow and CO2 sequestration in Kansas. AAPG Bull. 89, 1607–1627.

Chadwick, A., Arts, R., Eiken, O., Williamson, P., Williams, G., 2006. Geophysical monitoring of the CO_2 plume at Sleipner, North Sea: an outline review. In: Lombardi, S.E.B.S., Altunina, L.K. (Eds.), Advances in the Geological Storage of CarbonDioxide. Springer Dordrecht, The Netherlands, pp. 303–314.

Chahal, R., Starecki, F., Boussard-Plédel, C., Doualan, J.-L., Michel, K., Brilland, L., Braud, A., Camy, P., Bureau, B., Nazabal, V., 2016. Fiber evanescent wave spectroscopy based on IR fluorescent chalcogenide fibers. Sens. Actuators B: Chem. 229, 209–216.

Chan, K.L.A., Niu, X., de Mello, A.J., Kazarian, S.G., 2010. Rapid prototyping of microfluidic devices for integrating with FTIR spectroscopic imaging. Lab Chip 10, 2170–2174.

Chang, Y.-C., Wagli, P., Paeder, V., Homsy, A., Hvozdara, L., van der Wal, P., Di Francesco, J., de Rooij, N.F., Herzig, H.P., 2012. Cocaine detection by a mid-infrared waveguide integrated with a microfluidic chip. Lab Chip 12, 3020–3023.

Charlton, C., Katzir, A., Mizaikoff, B., 2005. Infrared evanescent field sensing with quantum cascade lasers and planar silver halide waveguides. Anal. Chem. 77, 4398–4403.

Charpentier, F., Starecki, F., Doualan, J.L., Jóvári, P., Camy, P., Troles, J., Belin, S., Bureau, B., Nazabal, V., 2013. Mid-IR luminescence of Dy^{3+} and Pr^{3+} doped $Ga_5Ge_{20}Sb_{10}S(Se)_{65}$ bulk glasses and fibers. Mater. Lett. 101, 21–24.

Charrier, J., Brandily, M.L., Lhermite, H., Michel, K., Bureau, B., Verger, F., Nazabal, V., 2012. Evanescent wave optical micro sensor based on chalcogenide glass. Sens. Actuators B-Chem. 173, 468–476.

Couto, R., Chambon, S., Aymonier, C., Mignard, E., Pavageau, B., Erriguible, A., Marre, S., 2015. Microfluidic supercrictical antisolvent continuous processing and direct spray-coating of poly3hexylthiophene nanoparticles for OFET devices. Chem. Commun. 51, 1008–1011.

Dochow, S., Becker, M., Spittel, R., Beleites, C., Stanca, S., Latka, I., Schuster, K., Kobelke, J., Unger, S., Henkel, T., Mayer, G., Albert, J., Rothhardt, M., Krafft, C., Popp, J., 2013. Raman-on-chip device and detection fibres with fibre Bragg grating for analysis of solutions and particles. Lab Chip 13, 1109–1113.

Duncombe, T.A., Tentori, A.M., Herr, A.E., 2015. Microfluidics: reframing biological enquiry. Nat. Rev. Mol. Cell. Biol. 16, 554–567.

El-Ali, J., Sorger, P.K., Jensen, K.F., 2006. Cells on chips. Nature 442, 403–411.

Eyal, O., Scharf, V., Shalem, S., Katzir, A., 1996. Single mode mid-infrared silver halide planar waveguides. Opt. Lett. 21, 1147–1149.

Ganjoo, A., Jain, H., Yu, C., Irudayaraj, J., Pantano, C.G., 2008. Detection and fingerprinting of pathogenes: mid-IR biosensor using amorphous chalcogenide films. J. Non-Cryst. Solids 354, 2757–2762.

Gunda, N.S.K., Bera, B., Karadimitriou, N.K., Mitra, S.K., Hassanizadeh, S.M., 2011. Reservoir-on-a-chip: a new paradigm in reservoir engineering. Lab Chip 11, 3785–3792.

Hale, G.M., Querry, M.R., 1973. Optical constants of water in the 200-nm to 200-μm wavelength region. Appl. Opt. 12, 555–563.

Hartman, R.L., Jensen, K.F., 2009. Microchemical systems for continuous flow synthesis. Lab Chip 9, 2495–2507.

Hingerl, F.F., Marpu, S., Guzman, N., Benson, S.M., Delgado-Alonso, J., 2014. Development and testing of a new fiber optic system for monitoring CO2 solublity in aqueous high-pressure geological systems. Energy Procedia 63, 4134–4144.

Jensen, K.F., Reizman, B.J., Newman, S.G., 2014. Tools for chemical synthesis in microsystems. Lab Chip 14, 3206–3212.

Kim, S.-S., Young, C., Mizaikoff, B., 2007. Miniaturized mid-infrared sensor technologies. Anal. Bioanal. Chem. 390, 231–237.

Kise, D.P., Magana, D., Reddish, M.J., Dyer, R.B., 2014. Submillisecond mixing in a continuous-flow, microfluidic mixer utilizing mid-infrared hyperspectral imaging detection. Lab Chip 14, 584–591.

Kubat, I., Rosenberg Petersen, C., Møller, U.V., Seddon, A., Benson, T., Brilland, L., Méchin, D., Moselund, P.M., Bang, O., 2014. Thulium pumped mid-infrared 0.9–9 μm supercontinuum generation in concatenated fluoride and chalcogenide glass fibers. Opt. Express 22, 3959–3967.

Liu, N., Aymonier, C., Lecoutre, C., Garrabos, Y., Marre, S., 2012. Microfluidic approach for studying CO2 solubility in water and brine using confocal Raman spectroscopy. Chem. Phys. Lett. 551, 139–143.

Lu, R., Li, W.W., Katzir, A., Raichlin, Y., Yu, H.Q., Mizaikoff, B., 2015. Probing the secondary structure of bovine serum albumin during heat induced denaturation using mid-infrared fiberoptic sensor. Analyst 140, 765–770.

Lucier, A., Zoback, M., 2008. Assessing the economic feasibility of regional deep saline aquifer CO2 injection and storage: a geomechanics-based workflow applied to the Rose Run sandstone in Eastern Ohio, USA. Int. J. Greenh. Gas Control 2, 230–247.

Ma, P., Choi, D.-Y., Yu, Y., Yang, Z., Vu, K., Thach, N., Mitchell, A., Luther-Davies, B., Madden, S., 2015. High Q factor chalcogenide ring resonators for cavity-enhanced MIR spectroscopic rings. Opt. Express 23, 19969–19979.

Marre, S., Jensen, K.F., 2010. Chem. Soc. Rev. 39, 1183–1202.

Marre, S., Aymonier, C., Subra, P., Mignard, E., 2009. Dripping to jetting transitions observed from supercrictical fluid in liquid micro coflows. Appl. Phys. Lett. 95, 134105.

Marre, S., Adamo, A., Basak, S., Aymonier, C., Jensen, K.F., 2010. Design and packaging of microreactors for high pressure and high temperature applications. Ind. Eng. Chem. Res. 49, 11310–11320.

Moizan, V., Nazabal, V., Troles, J., Houizot, P., Adam, J.-L., Doualan, J.-L., Moncorgé, R., Smektala, F., Gadret, G., Pitois, S., Canat, G., 2008. Er^{3+}-doped GeGaSbS glasses for mid-IR fibre laser application: synthesis and rare earth spectroscopy. Opt. Mater. 31, 39–46.

Morais, S., Liu, N., Diouf, A., Bernard, D., Lecoutre, C., Garrabos, Y., Marre, S., 2016. Monitoring CO_2 invasion processes at the pore scale using geological labs on chip. Lab Chip 16, 3493–3502.

Mori, C., Sato, T., Kano, Y., Oyama, H., Aleynik, D., Tsumune, D., Maeda, Y., 2015. Numerical study of the fate of CO2 purposefully injected into sediment and seeping from the seafloor in Ardmucknish bay. Int. J. Greenh. Gas Control 38, 153–161.

Pan, T., Kelly, R.T., Asplund, M.C., Woolley, A.T., 2004. Fabrication of calcium fluoride capillary electrophoresis microdevices for on-chip infrared detection. J. Chromatogr. A 1027, 231–235.

Pelé, A.L., Braud, A., Doualan, J.L., Chahal, R., Nazabal, V., Boussard-Plédel, C., Bureau, B., Moncorgé, R., Camy, P., 2015. Wavelength conversion in Er^{3+} doped chalcogenide fibers for optical gas sensors. Opt. Express 23, 4163–4172.

Perrin, J.-C., Krause, M., Kuo, C.-W., Milikovic, L., Charoba, E., Benson, S.M., 2009. Characterization of CO_2 storage properties using core analysis techniques and thin selection data. Energy Procedia 1, 3515–3522.

Perro, A., Lebourdon, G., Henry, S., Lecomte, S., Servant, L., Marre, S., 2016. Combining microfluidics and FT-IR spectroscopy: towards spatially resolved information on chemical processes. React. Chem. Eng.

Quieros, A.M., Taylor, P., Cowles, A., Reynolds, A., Widdicombe, S., Stahl, H., 2015. Optical assessement of impact and recovery of sedimentary pH profiles in ocean acidification and carbon capture and storage research. Int. J. Greenh. Gas Control 38, 110–120.

Sanghera, J.S., Shaw, L.B., Aggarwal, I.D., 2009. Chalcogenide glass-fiber-based mid-IR sources and applications IEEE. J. Sel. Top. Quantum Electron. 15, 114–119.

Singh, V., Lin, P.T., Patel, N., Lin, H.T., Li, L., Zou, Y., Deng, F., Ni, C.Y., Hu, J.J., Giammarco, J., Soliani, A.P., Zdyrko, B., Luzinov, I., Novak, S., Novak, J., Wachtel, P., Danto, S., Musgraves, J.D., Richardson, K., Kimerling, L.C., Agarwal, A.M., 2014. Mid infrared materials and devices on a Si platform for optical sensing. Sci. Technol. Adv. Mater. 15, 014603.

Starecki, F., Charpentier, F., Doualan, J.-L., Quetel, L., Michel, K., Chahal, R., Troles, J., Bureau, B., Braud, A., Camy, P., Moizan, V., Nazabal, V., 2015. Mid-IR optical sensor for CO_2 detection based on fluorescence absorbance of Dy^{3+}:$Ga_5Ge_{20}Sb_{10}S_{65}$ fibers. Sens. Actuators B: Chem. 207 (Part A), 518–525.

Wagner, C., Buchegger, W., Vellekoop, M., Kraft, M., Lendl, B., 2011. Time-resolved mid-IR spectroscopy of biochemical reactions in solution utilizing a new generation of continuous flow micro-mixers. Anal. Bioanal. Chem. 400, 2487–2497.

Yue, J., Falke, F.H., Schouten, J.C., Nijhuis, T.A., 2013. Microreactors with integrated UV/Vis spectroscopic detection for online process analysis under segmented flow. Lab Chip 13, 4855–4863.